N85-22488

WAKES AND DIFFERENTIAL CHARGING OF LARGE BODIES IN LOW EARTH ORBIT

Lee W. Parker
Lee W. Parker, Inc.
Concord, Massachusetts 01742

Highlights of earlier results by the author and others using the author's Inside-Out WAKE code on wake structures of LEO spacecraft are reviewed. For conducting bodies of radius large compared with the Debye length (large inverse Debye number), a high-Mach-number wake develops a negative potential well. Quasineutrality is violated in the very near wake region, and the wake is relatively "empty" for a distance downstream of about one-half of a "Mach number" of radii. There is also a suggestion of a core of high density along the axis. We report recent work on very large bodies in LEO.

A comparison of rigorous numerical solutions with in-situ wake data from the AE-C satellite suggests that the so-called "neutral approximation" for ions (straight-line trajectories, independent of fields) may be a reasonable approximation except near the center of the near wake. This approximation is adopted here for very large bodies.

In an earlier investigation of differential charging of small nonconducting bodies due to plasma flows, it was found that the scale of the voltage difference between the upstream and downstream surfaces ("front" and "wake" surfaces of a nonconducting body) due to a high-Mach-number plasma flow is governed by the ion drift energy. Hence kilovolt potential differences may occur in the solar wind, for example, between a spacecraft and a piece of insulated material in its near wake.

Recent work has concerned the "wake-point" potential of very large nonconducting bodies such as the Shuttle Orbiter. Using a cylindrical model for bodies of this size or larger in LEO (body radius up to 10^5 Debye lengths), approximate solutions are presented based on the neutral approximation(but with rigorous trajectory calculations for surface current balance). There is a negative potential well if the body is conducting, and no well if the body is nonconducting. In the latter case the wake surface itself becomes highly negative. The wake-point potential is governed by the ion drift energy.

LARGE-BODY WAKE STRUCTURE: CONDUCTING BODIES

Parker's wake-theory computer model for pillbox shapes (Inside-Out Method for warm ions - see refs. 1-3) was applied by the author and others in a number of wake calculations. High-voltage sheaths and wakes of large bodies require special numerical techniques (see refs. 3 and 12 for generalization to 3-D geometries, CLEPH code).

Wake of Moderately-Large Conducting Body in LEO

First we present highlights of earlier results obtained (1976, see refs. 1-2) in a problem involving the wake of a large body in LEO, 100 Debye lengths in radius. The body is in the form of a disk oriented normal to the flow. For two cases (figs. 1a and 1b) the parameter values are:

Case 1			Case 2
ϕ_o	$= -4$	(dimensionless potential in units of kT/e)	$\phi_o = -4$
λ_D^{-1}	$= 100$	(inverse Debye number = ratio of body radius to Debye length)	$\lambda_D^{-1} = 100$
M	$= 4$	(ion Mach number)	M $= 8$

This size of moving body is larger than had been treated prior to 1976 by trajectory-following, i.e., realistic, calculations. The results show what may be expected for the wake structure of large bodies in general. The problem of a large body requires more effort (computer time and judicious selection of numerical parameters) than that of a smaller body. The solutions shown, therefore, are intended to be illustrative rather than accurate. The Inside-Out Method was used (refs. 1-3).

Poisson-Vlasov iteration was applied (refs. 1,2), starting with the neutral-approximation ion density as an initial guess. A nominal number of trajectories, 512, was used at all grid points. The grid is similar to fig. 2a with z>0.

The profiles of n_i, n_e, and ϕ (dimensionless ion density, electron density and potential) are shown in figure 1a for Case 1. Tabulated values are given in reference 2. The wake is essentially "empty" of both ions and electrons between z=0 and z=1, and begins to fill up between z=2 and z=3, where z denotes the distance downstream in units of the body radius.

Two sets of ion-density profiles are shown on the left side of figure 1a, the unlabeled profiles for the final iteration, and the profiles labeled "A" for the previous iteration. Comparison of the n_e-profiles with the n_i-profiles labeled "A" (to denote that the ϕ-profiles and n_e-profiles in the figure are derived from these) indicates that the quasineutrality assumption is valid everywhere outside a cone-shaped region near the wake surface; the cone height along the axis is between one and two radii. This is in accord with expectation for a large body. Near the wake surface, however, quasineutrality is violated because the effective Debye length is large. The similarity of the n_i-profiles labeled "A" and the n_e-profiles in figure 1a is a consequence of near-quasineutrality.

Despite possible inaccuracies, one may infer certain physical conclusions from figure 1a, namely, (a) the suggestion of a core of high (approximately ambient) density of ions and electrons on the axis, and (b) the occurrence of a potential well in the near wake, defined as a region with ϕ-values below -4. The shading in the two lowest ϕ-profiles denote cross sections of this well. The wake-surface normalized fluxes are 1.1×10^{-8} ("A") and 2.4×10^{-7} (final) for ions, and 4.3×10^{-3} for electrons. The electron current density is less than $\exp(-4)$, as would be expected in the presence of a potential well.

The region of wake disturbance probably extends more than 6 radii downstream, and between 2 and 3 radii in the transverse direction.

Case 2 (fig. 1b) is similar to Case 1 except that the Mach number is increased from M=4 to M=8. The next-to-final and final-order ion densities are labeled "A" and unlabeled, respectively. On comparing these, the convergence seems fairly good at z=0.5 and z=1 radii downstream. Again, the disturbance extends beyond z=5, so that the downstream boundary should be moved further than z=6 radii downstream.

Despite possible inaccuracies, the consistency is such that physical conclusions may be drawn as follows. In this case the wake is seen to remain empty further downstream than in the M=4 case. In addition, the suggestion is much stronger that there is a central core of ambient density for both ions and electrons along the axis. Moreover, the potential well is wider and longer than in the M=4 case, although the depth is about the same. The normalized wake-surface fluxes are 7.4×10^{-30} ("A") and 4.2×10^{-30} (final) for ions, and 3.7×10^{-3} for electrons. The electron flux is slightly less than the M=4 value, and is again less than exp(-4).

The conical region behind the disk where quasineutrality breaks down is now longer than in the M=4 case, extending to between z=4 and z=5 radii along the axis.

The region of wake disturbance is probably longer than 6 radii downstream, as in the M=4 case, but may not extend beyond about 2 radii in the transverse direction.

Theory-Experiment Comparison for AE-C Satellite

Next, we note that Parker's wake theory computer model has been applied by Samir and Fontheim (ref. 4) in a comparative study of ion and electron distributions in the wakes of ionospheric satellites. From a comparison between the theory and ion measurements on the AE-C satellite, Samir and Fontheim show that theory and experiment agree fairly well in the "angle-of-attack" range between 90° and 135°. (The upstream and downstream directions are defined by 0° and 180°, respectively.) A significant finding is the fact that in that angular range even the "neutral approximation" for ions (straight-line trajectories, independent of electric fields) gives fair agreement with the measurements. (In the near-wake maximum rarefaction zone near 180°, both the neutral approximation and the self-consistent solution underestimate the measured ion densities - inferred from probe currents - by orders of magnitude. Electron data obtained by the Explorer 31 satellite also shows an underestimation near 180° by the Parker wake theory, although less pronounced.)

The largest ratio of body-radius-to-Debye-length (that is, the inverse of the Debye number) treated by Samir and Fontheim (ref. 4) is R_D=162, in one of the AE-C cases.

Figures 2a, b (from ref. 4) illustrate the geometry of the AE-C ion measurement, and the ion results for inverse Debye number 162. The locations of the ion current observation points, and of the numerical grid points at which densities were calculated, are shown in figure 2a. The geometry of the theoretical model is that of a pillbox cylinder with its axis parallel to the flow, while the true geometry is that of a pillbox cylinder in a "cross-flow," that is, with its axis perpendicular to the flow. In spite of this, the theory-experiment comparison is deemed by Samir and Fontheim to be meaningful, in view of uncertainties in the calculations and estimated measurement errors. (The depth in the direction of the flow is the same for both the satellite and the model, and the cross sections presented to the flow are nearly the same.) The current probe moves on a circular arc at a radial distance of about 1.5 satellite radii.

In figure 2b, the measured angular profile is shown together with the neutral approximation (zero-th iteration) and the self-consistent solution (15-th iteration). The self-consistent solution is closer to the experimental profile, in the angular range 90° - 147°, than the neutral approximation. Near 180°, the self-consistent solution is 2 to 3 orders of magnitude below the measured data, while the neutral approximation is about 10 orders of magnitude lower.

However, in their overall comparison assessment, Samir and Fontheim state that the neutral approximation describes the observed profiles more and more accurately as the inverse Debye number (ratio of body radius to Debye length) becomes large. This is justified physically based on the expectation that charge separation effects become weaker as the body size increases. This is equivalent to the setting-in of the quasineutrality regime, at sufficiently large inverse Debye numbers.

Wake of Very Large Conducting Body in LEO: Recent Results

We now treat the wake of a much larger conducting body, larger than any treated previously. In this case the self-consistent calculation becomes computationally relatively expensive. However, a reasonable approximation is afforded through the use of the "neutral approximation" for ions. That is, the ion trajectories governing ion space charge density are treated as if the ions were uncharged and unaffected by the field. The electron space charge density is assumed to be given by the "Boltzmann factor", that is, the exponential of the repulsive dimensionless potential. To some extent this approximation is supported by the Samir and Fontheim in-situ comparison discussed above. In any case it is qualitatively valuable and leads to physical insights with a minimum of computational expense. This approximation was used by Kiel et al (ref. 11). (We compute current balance later using rigorous trajectories.)

The potential distribution in the wake of a conducting satellite, in the form of a long cylinder with its axis normal to the flow, assumed to have a dimensionless potential of 3 kT/e, is shown in figures 3a, b and c, for bodies with inverse Debye numbers ranging from 10 to 10^5, and flow Mach numbers 2, 5 and 8. Figure 3a shows how the wake potential profile varies with inverse Debye number, for fixed Mach number = 8. The profiles for inverse Debye numbers 10, 10^2 and 10^3 are similar to results obtained earlier for a sphere by Kiel et al (see fig. 5 of ref. 11). The Kiel et al (ref. 11) results are for inverse Debye numbers up to 10^3. We have extended the solutions to 10^5. The wake potential profile has a negative minimum for inverse Debye numbers greater than about 10. The magnitude of the minimum is about 7, 10, 14 and 19, respectively, for inverse Debye numbers 10^2, 10^3, 10^4 and 10^5. Figure 3b shows how the wake potential profile varies with Mach number, for fixed inverse Debye number = 10^5. The depth of the potential minimum clearly increases with both increasing Mach number and inverse Debye number. Figure 3c shows equipotential contours for Mach number = 8 and inverse Debye number = 10^5.

These results would be applicable to the Shuttle Orbiter (inverse Debye number about 10^4) if it were a conducting body. However, most of its surface (about 97%) is covered with nonconducting tiles. Hence it must be treated as a large nonconducting body in LEO. The differential charging of such bodies is treated in the remainder of this paper.

WAKE STRUCTURES AND DIFFERENTIAL CHARGING OF SMALL AND LARGE NONCONDUCTING BODIES DUE TO PLASMA FLOWS

Differential Charging

Differential spacecraft charging takes place when the spacecraft surface is partly or entirely insulating and the charged-particle fluxes vary from point to point over the surface. In the familiar case of photoelectric emission from a sunlit insulated area, due to electrons escaping from it the sunlit area tends to become positively charged relative to the surrounding dark areas (refs. 5-7). Another mechanism of differential charging, which is less familiar and appears to have been treated only very recently (ref. 8), is that due to the relative motion between a nonconducting spacecraft and the external plasma (e.g., a spacecraft in the ionosphere or in the solar wind). The fluxes of ambient ions and electrons on the wake surface are not the same as on the front surface. For high velocities of relative motion compared with the mean ion thermal velocity, whether this occurs in the ionosphere (due principally to spacecraft motion) or in the solar wind (due principally to plasma motion), there is a significant differential in the ion fluxes, but a negligible differential for the electrons. Since the net current density must vanish locally at each surface point in the steady state, this plasma-flow effect leads to a larger negative equilibrium potential on the wake surface than on the front surface. If there is photoemission as well on the front surface (as in the solar wind), this differential charging is enhanced. As shown below, this plasma-flow effect can generate differences between the front and wake surface potentials amounting to many kT/e (where T is the temperature, k is Boltzmann's constant, and e is the electron charge), together with a potential barrier for electrons. The potential difference can be expected to be of the order of volts in the ionosphere, and one kilovolt in the solar wind, that is, of the order of the ion drift energy (ref. 8).

Even weak differential charging can interfere with measurements of, say, weak ambient electric fields or low-energy particle spectra, and it can create electron potential barriers which can return emitted photoelectrons or secondary electrons to the surface and lead to erroneous interpretations of the data (ref. 9). This type of electron potential barrier is distinct from, and should not be confused with, the more familiar space-charge potential minimum which can be produced by emitted-electron space charge (ref. 10) and is not due to differential charging. The barrier produced by differential charging effects may be more important than the potential minimum caused by space charge.

The next section results show what may be expected: (a) in the ionosphere for small insulated objects, small meteroids, or small parts of a spacecraft (e.g., a painted antenna) located within the wake region of a moving spacecraft, and (b) in the solar wind for an entire spacecraft, or small natural bodies in the solar system. Following the next section, the wake structure and differential charging of very large nonconducting bodies in Low Earth Orbit will be treated.

Differential Charging of Small Nonconducting Body

In the problem treated next (see fig. 4), we assume the nonconducting spacecraft to have a "pillbox" shape, and to be in a flowing plasma, with the plasma flow along the axis, from the "front" region toward the "wake" region. The plasma is taken to be ionized hydrogen and is assumed to have a velocity of flow 4 times larger than the most probable ion thermal velocity (ion "Mach number" = 4). (In the solar wind, this Mach number would be approximately 10.) Since the unperturbed ion flux to the wake surface is about 9 orders of magnitude smaller than the corresponding ion flux to the front surface, and since the electron fluxes are about the same to the front and wake surfaces, there will be a significant differential between the equilibrium potentials at the front and wake surfaces (see below).

Using the Inside-Out Method, current densities of ions and electrons are evaluated at many points on the spacecraft surface (refs. 7-8). The local surface potentials were varied until current balance was achieved at each point.

Figure 4 shows equipotential contours around the spacecraft, obtained by numerical solution, labeled by numbers representing dimensionless values of the potential (in units of kT/e, where T is the plasma temperature, and assuming $T_i = T_e$). These potentials are obtained from Laplace's equation (space charge negligible for small bodies), where the surface potentials are obtained by the relaxation method discussed by Parker (ref. 8), under the requirement of zero net current density at all surface points. The errors in the solution shown are estimated to be under 10 percent, based on several runs giving similar answers starting from different initial guesses.

There are three regions of characteristic behavior of the potential: the "wake", the "side", and the "front". Near the "wake point," the potentials are of the order of −10 kT/e. This large negative value is associated with the reduction in ion flux due to the flow. In the side region the potentials are of the order of −3 kT/e; this is essentially the order of the equilibrium potential when there is no flow ($\sim -(kT/e)\ln(m_i/m_e)^{\frac{1}{2}}$). In the front region the potentials are of the order of −kT/e, i.e., are less negative than those on the side, because of the enhancement of the ion flux due to the flow. (Adding photoemission here would make the front potential still less negative.) The surface points are thus not equipotential. Note that there is a saddle point in the front region, that is, a potential barrier for electrons. This feature is caused by the interaction between the relatively large magnitude wake-point potentials and the relatively low magnitude front potentials. The dashed part of the contour labeled "−3.0" near the side surface indicates that there is more complicated fine structure (variation of potential along the side surface) than is shown in the figure. The potentials along the wake surface fall off toward the corner. The potentials along the front surface first fall with radius and then rise sharply as the corner is approached. This may be a "corner effect."

It is shown by Parker (ref. 7) that when the ion Mach number is large (in the ionosphere and solar wind), the potential difference ΔV generated by the flow should be of the order of $m_i v^2/2e$, or $0.0052 m_i(\text{amu}) v^2(\text{km/s})$ in volts, where $m_i(\text{amu})$ and $v(\text{km/s})$ denote the ion mass in atomic mass units and the flow velocity in kilometers per second, respectively. In the ionosphere, with oxygen ions and orbital velocities of the order of 8 km/s, ΔV is about 5 V. Hence one would expect a relatively small body in the ionosphere, such as a thin antenna or boom painted with nonconducting paint, or a painted or insulated object in the very near wake of a spacecraft (or the spacecraft surface itself if it is a dielectric) to become highly negatively charged to potentials of the order of volts in the ionosphere.

In the solar wind these results could apply to an entire spacecraft, since it is small in comparison with the Debye length. With protons and solar wind velocities of about 400 km/s or higher, ΔV is of the order of 1 kV. This means that one may have kilovolt potential differences between the wake and front surfaces. The electric fields due to this differential charging may significantly disturb measurements of space electric fields, or of low-energy plasma electrons, for example, on the Helios spacecraft (ref. 6). Moreover, because of this solar wind flow effect, small natural bodies in the solar system (i.e., bodies not large in comparison with the Debye length or ion gyroradius) may be expected to become differentially charged with potential differences of the order of 1 kV, independent of whether there is photoemission or not. Candidates for this effect include micrometeroids, dust, asteroids, the planet Pluto, and natural small satellites such as Mars' moon Deimos and Saturn's ring material when they are outside the bow shock (M. Dryer, personal communication, 1978).

For large bodies in flowing plasmas, space charge cannot be neglected. The wakes and differential charging of very large bodies are treated in the following section.

Wake Structure and Differential Charging of Very Large Nonconducting Bodies in LEO Plasma Flows: Recent Results

There is considerable interest in the charging and electric fields of the Shuttle Orbiter. This is an important example of a very large spacecraft in Low Earth Orbit (inverse Debye number about 10^4) with most of its surface (about 97%) nonconducting. Only the small area in the vicinity of the engines is conducting and electrically grounded to the main frame. Figures 5a and 5b indicate how the Orbiter may be subjected to different types of differential charging depending on its orientation with respect to the plasma-flow direction. In figure 5a, the Orbiter is moving "nose-forward," i.e.. heading into the flow. The wake-point potential (location indicated by a cross) occurs essentially in the engine area, and thus defines also the Orbiter's ground potential. The rest of the spacecraft surface is electrically isolated and has in general a different potential distribution. The cargo bay area is a "side" region according to the terminology of the previous section. In figure 5b the Orbiter is moving "belly-forward." With this orientation the wake-point potential occurs in the cargo bay area, which is electrically isolated from the Orbiter ground. The ground is defined by a different potential attained by the engine area. In the shown orientation, the engine area is a "side" region.

Hence, the maximum negative ground potential of the Orbiter would occur when the Orbiter is in the nose-forward orientation, while the cargo-bay potential would be intermediate between this and the plasma potential. With the belly-forward orientation, the roles of ground potential and cargo-bay potential would be reversed, with the cargo bay at maximum negative potential, and Orbiter ground at intermediate potential.

In the present paper the wake structure and the wake-point potential of a very large nonconducting body in LEO such as the Orbiter are calculated using certain approximations. The geometry is modeled by a circular cylinder as illustrated in figure 6. The wake point is the isolated area indicated by a cross in the figure. Again, because of computational expense, we use the neutral approximation, but only for ion space charge. However, the differential charging, e.g. the wake-point potential, is calculated rigorously by current balance using Inside-Out-Method trajectories (refs. 7-8), for both ions and electrons, in the resulting electric field distribution.

For a nonconducting body of any size, current balance at the wake point results in significant negative wake-surface potentials. (Nonconducting bodies were not treated by Kiel et al.) Figures 7a and 7b show results for inverse Debye number 10^5, and Mach numbers 2, 5 and 8. There is no potential minimum. Instead the wake point attains the highest negative potential, resulting in a monotonic rather than non-monotonic potential profile in the wake. Figure 7a shows how the wake-point potential increases with increasing Mach number, for a fixed inverse Debye number = 10^5. The wake-point potential magnitude is about 8, 20 and 36 kT/e, respectively, for Mach numbers 2, 5 and 8. Figure 7b shows equipotential contours for Mach number = 8 and inverse Debye number = 10^5. These contours (nonconducting body) may be compared with those of a large conducting body with the same parameters (fig. 3c).

Table 1 shows how the wake surface potential of a nonconducting large body varies with Mach number and inverse Debye number. Evidently, the wake surface potential is insensitive to inverse Debye number. The table also gives the values of the dimensionless current density (equal of course for ions and electrons) at the wake surface. For comparison, also shown are the ion currents that would result from using the neutral approximation to calculate currents (see ref. 7). These are seen to be many orders of magnitude smaller than the more realistic currents calculated using ion trajectories affected by the field.

For large nonconducting bodies in high-Mach-number flows, the wake-to-front potential difference generated by the flow is less than but of the order of the potential-equivalent of the ion drift energy. This result is similar to that obtained above for the case of a small nonconducting body.

Finally, we illustrate in figures 8a, 8b and 8c examples of intricate 3-D large-body geometries of aerospace interest (including the Orbiter) for which a wake-modeling capability will be achieved using techniques presently under development at Lee W. Parker, Inc.

REFERENCES

1. Parker, L. W.: Calculation of Sheath and Wake Structure About a Pillbox-Shaped Spacecraft in a Flowing Plasma. In Proceedings of the Spacecraft Charging Technology Conference, C. P. Pike and R. R. Lovell, eds., AFGL-TR-77-0051/ NASA TMX-73537, 1977, pp. 331-366.

2. Parker, L. W.: Computation of Collisionless Steady-State Plasma Flow Past a Charged Disk. NASA CR-144159, Lee W. Parker, Inc., Feb. 1976.

3. Parker, L. W.: Contributions to Satellite Sheath and Wake Modeling. In 17th ESLAB Symposium: Spacecraft-Plasma Interactions and Their Influence on Field and Particle Measurements, A Pedersen, ed., European Space Technology Center, Noordwijk, The Netherlands, 1983.

4. Samir, U. and Fontheim, E. G.: Comparison of Theory and In-Situ Observations for Electron and Ion Distributions in the Near Wake of the Explorer 31 and AE-C Satellites. Planet. Space Sci., vol. 29, 1981, pp. 975-987.

5. Grard, R. J. L.; Knott, K.; and Pedersen, A.: The Influence of Photoelectron and Secondary Electron Emission on Electric Field Measurements in the Magnetosphere and Solar Wind. In Photon and Particle Interactions with Surfaces in Space, R. J. L. Grard, ed., D. Reidel, Dordrecht, Netherlands, 1973, pp. 163-189.

6. Rosenbauer, H. R.: Possible Effects of Photoelectron Emission on a Low Energy Electron Experiment. In Photon and Particle Interactions with Surfaces in Space, R. J. L. Grard, ed., D. Reidel, Dordrecht, Netherlands, 1973, pp. 139-151.

7. Parker, L. W.: Potential Barriers and Asymmetric Sheaths Due to Differential Charging of Nonconducting Spacecraft. AFGL-TR-78-0045, Lee W. Parker, Inc., Jan. 1978.

8. Parker, L. W.: Differential Charging and Sheath Asymmetry of Nonconducting Spacecraft Due to Plasma Flows. J. Geophys. Res., vol. 83, 1978, pp. 4873-4876.

9. Fahleson, U.: Plasma-Vehicle Interactions in Space - Some Aspects of Present Knowledge and Future Development. In Photon and Particle Interactions with Surfaces in Space, R. J. L. Grard, ed., D. Reidel, Dordrecht, Netherlands, 1973, pp. 563-569.

10. Guernsey, R. L. and Fu, J. H. M.: Potential Distribution Surrounding a Photo-Emitting Plate in a Dilute Plasma. J. Geophys. Res., vol. 75, 1970, pp. 3193-3199.

11. Kiel, R. E.; Gey, F. C.; and Gustafson, W. A.: Electrostatic Potential Fields of an Ionospheric Satellite. AIAA J., vol. 6, 1968, pp. 690-694.

12. Parker, L. W.; Holeman, E. G.; and McCoy, J. E.: Sheath Shapes: A 3-D Generalization of the Child-Langmuir Sheath Model for Large High-Voltage Space Structures in Dense Plasmas. In Proceedings of the Air Force Geophysics Laboratory Workshop on Natural Charging of Large Space Structures in Near-Earth Polar Orbit: 14-15 September 1982, R. C. Sagalyn, D. E. Donatelli and I. Michael, eds., AFGL-TR-83-0046, 25 January 1983, pp. 337-389.

TABLE 1. WAKE-POINT POTENTIALS OF LARGE NONCONDUCTING BODIES IN PLASMA FLOWS

ϕ_{sw} = dimensionless potential magnitude on wake surface, in units of kT/e (ϕ_s = 3 at "side" surface)

M = Mach number

λ_D^{-1} = Inverse Debye number

J_{eo} = electron random thermal current density

J_e = electron current density (in units of J_{eo}). Rigorous trajectory analysis.

J_i = ion current density (in units of J_{eo}). Rigorous trajectory analysis.

J_{in} = neutral-approximation ion current density (in units of J_{eo})

$\sim (m_e/m_i)^{1/2} \exp(-M^2)/2M^2$ (ref. 7)

	M = 2	M = 5	M = 8
λ_D^{-1}	10 to 10^5	10 to 10^5	10 to 10^5
ϕ_{sw}	~ 8	~ 20	~ 40
$J_i = J_e$	$\sim 10^{-4}$	$\sim 10^{-8}$	$\sim 10^{-16}$
J_{in}	$\sim 10^{-5}$	$\sim 10^{-15}$	$\sim 10^{-32}$

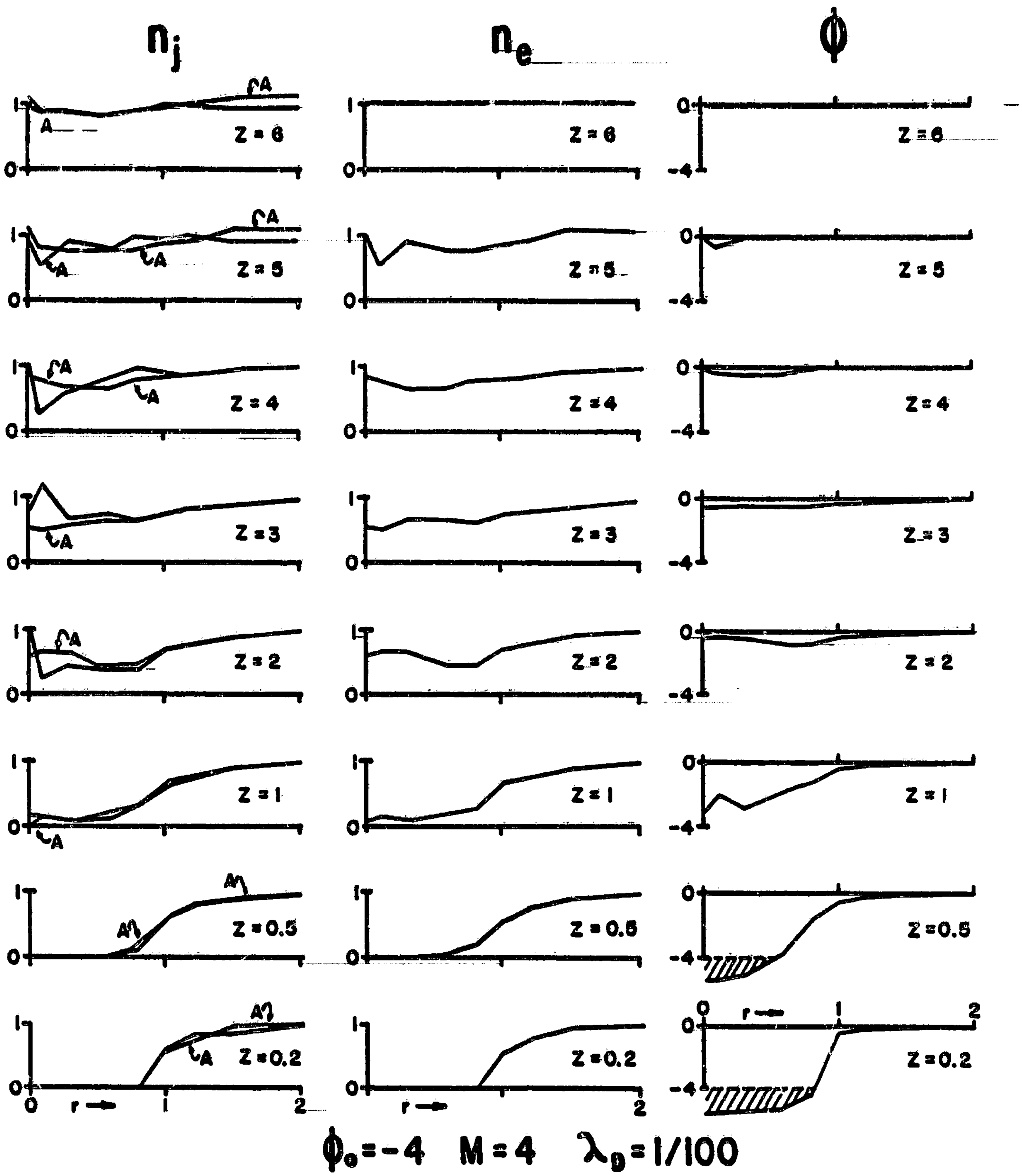

(a) M=4.

Figure 1. - Large-body wake profiles. Conducting disk with 4 kT/e surface potential.

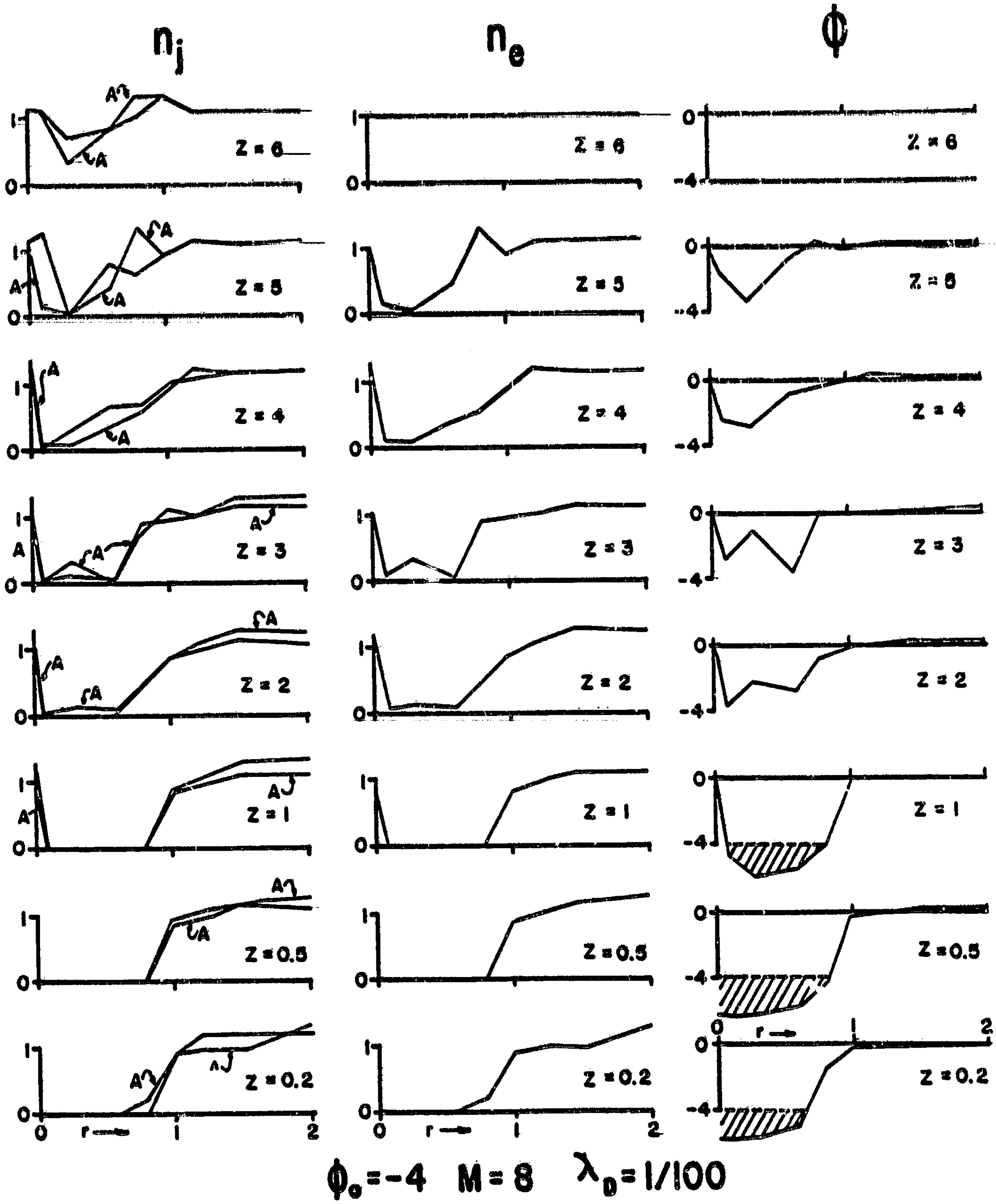

(b) M=8.

Figure 1. - Concluded.

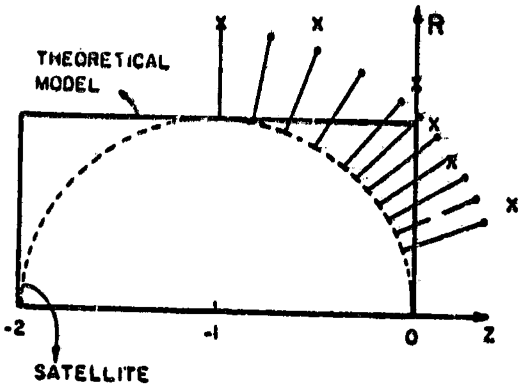

(a) Theoretical model (solid) versus real satellite geometry (dotted). (Dots denote ion current observation points; X's denote numerical grid points at which densities are calculated.)

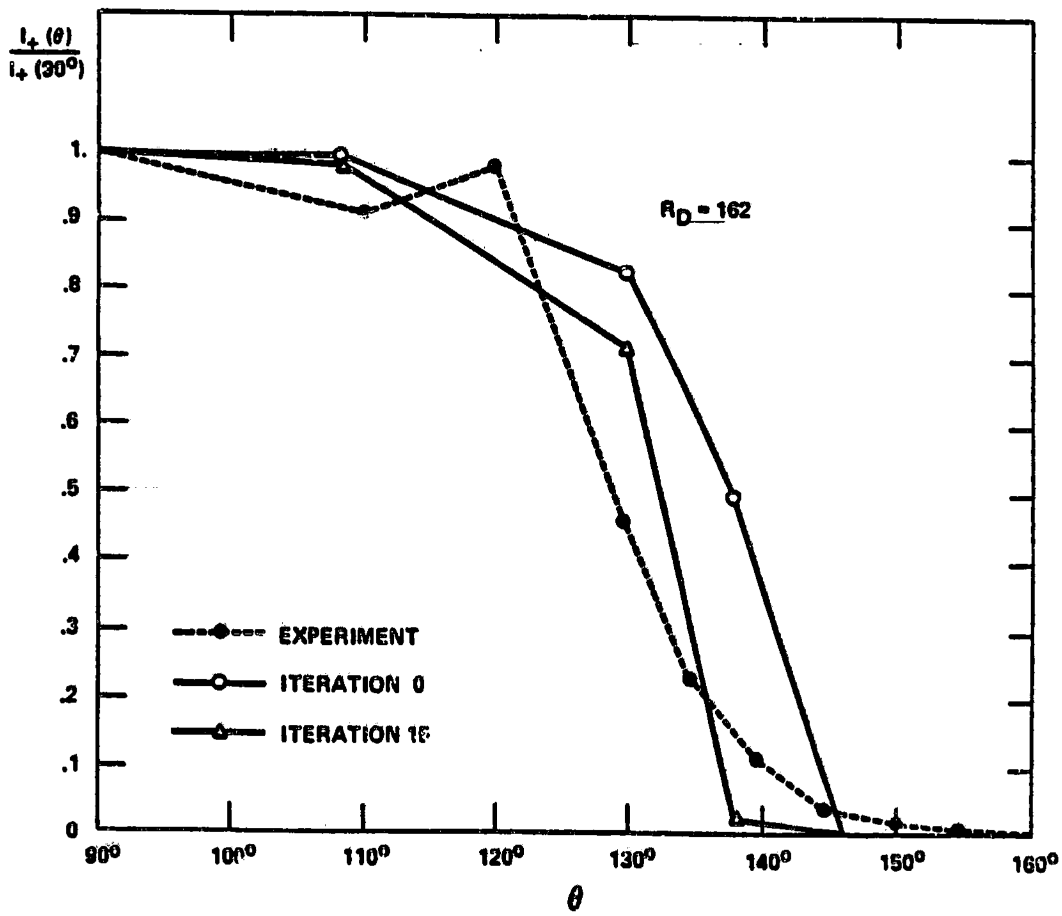

(b) Measured angular profile on AE-C satellite (large body; 162 Debye lengths) compared with neutral-approximation theory (iteration zero) and self-consistent theory (iteration 15).

Figure 2. - Geometry of AE-C ion measurements.

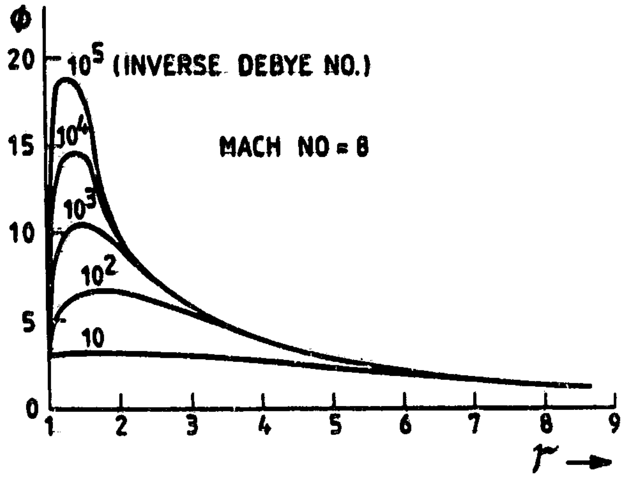

(a) Variation with inverse Debye number at fixed Mach number = 8.

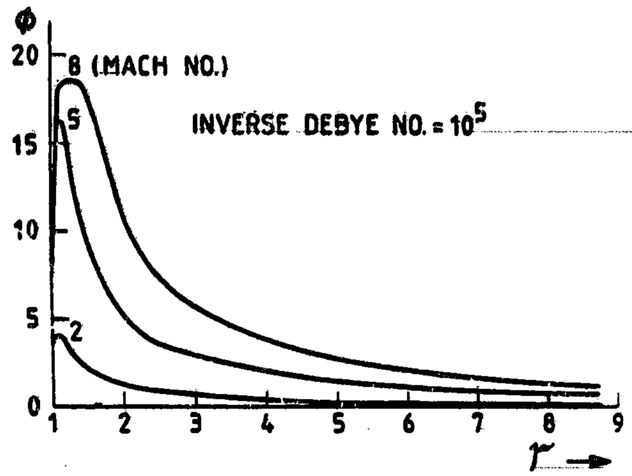

(b) Variation with Mach number, at fixed inverse Debye number = 10^5.

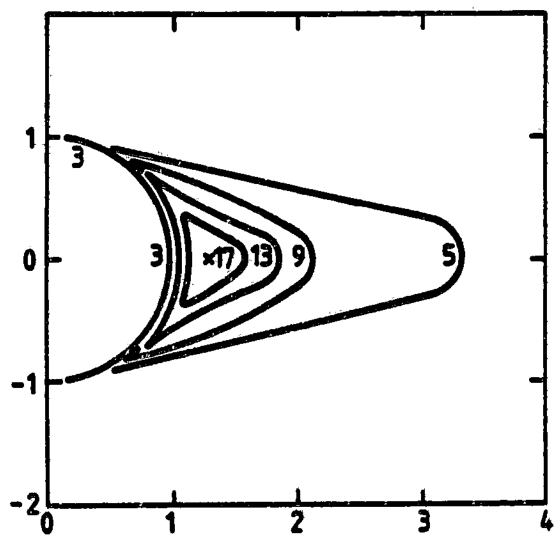

(c) Equipotential contours. Mach number = 8. Inverse Debye number = 10^5. (The point marked "x" is the position of peak potential = 19; dimensions in units of spacecraft radius.)

Figure 3. - Wake potential profiles (dimensionless potential) and equipotential contours in wake of conducting cylinder with 3 kT/e surface potential. ϕ = potential in units of kT/e; r = downstream distance in units of spacecraft radius.

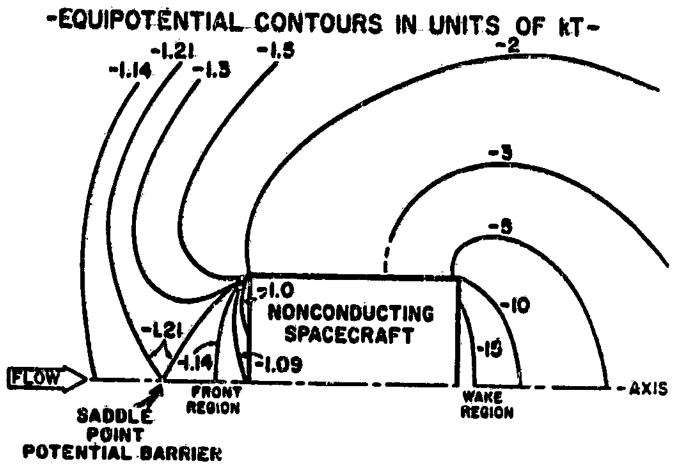

Figure 4. - Differential charging of nonconducting spacecraft in plasma flow at Mach 4. No space charge.

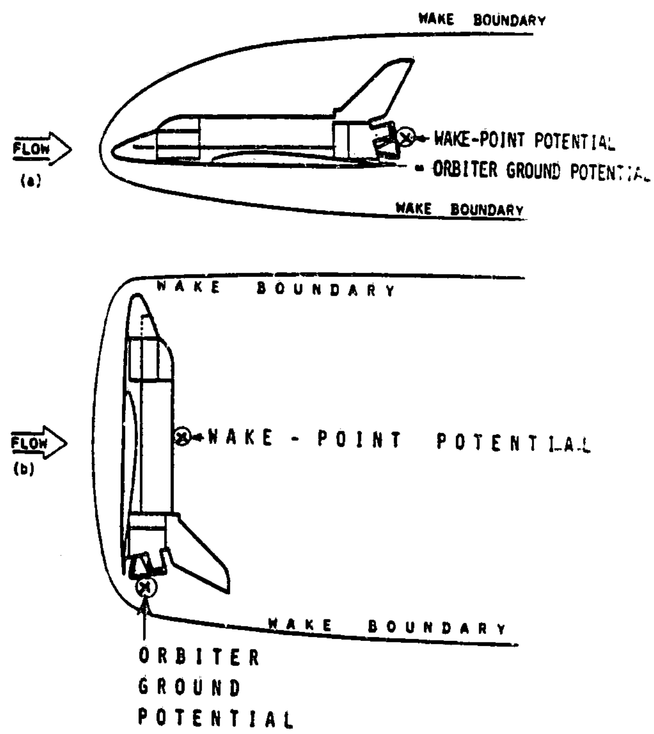

(a) Nose-forward orientation.

(b) Belly-forward orientation.

Figure 5. - Shuttle orbiter in LEO plasma flow, indicating wake points and orbiter ground potential points. Very large nonconducting body.

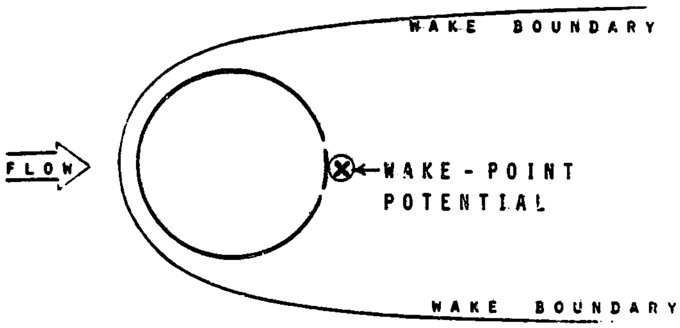

Figure 6. - Very large nonconducting cylinder model of shuttle orbiter in LEO plasma flow, indicating wake point.

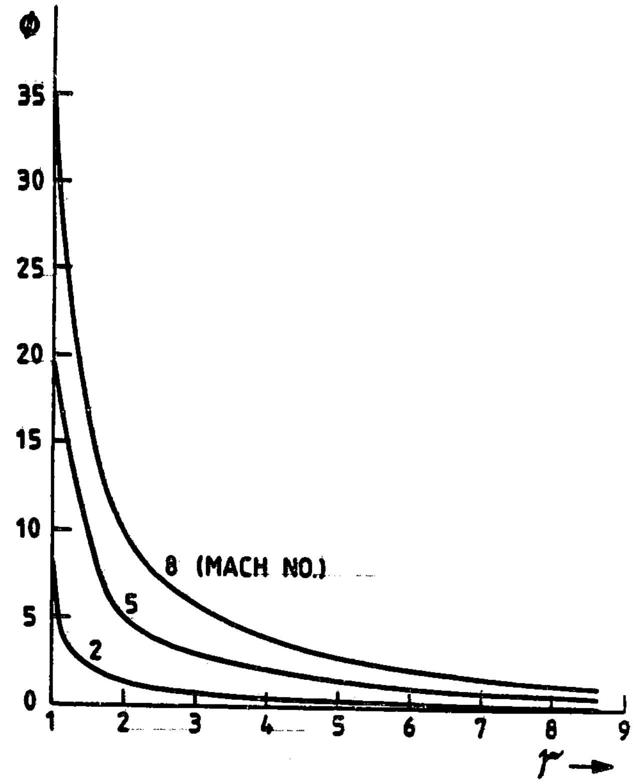

(a) Variation with Mach number at fixed inverse Debye number of 10^5.

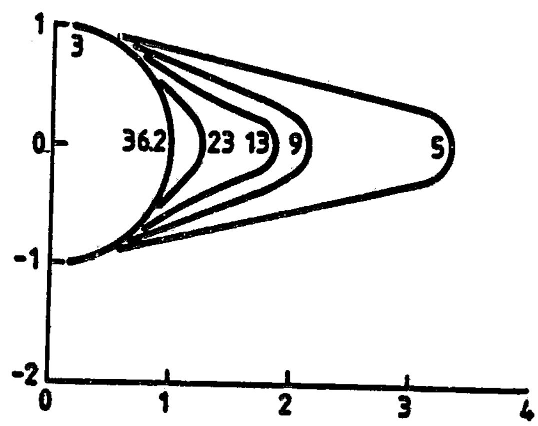

(b) Equipotential contours (dimensionless potential) in wake of nonconducting cylinder. Surface potential distribution from 3 to 36.2, in units of kT/e, determined by pointwise current balance. Mach number = 8. Inverse Debye number = 10^5. (Dimensions in units of spacecraft radius).

Figure 7. - Wake potential profiles (dimensionless potential and equipotential contours in wake of nonconducting cylinder. ϕ = potential in units of kT/e; r = downstream distance in units of spacecraft radius.

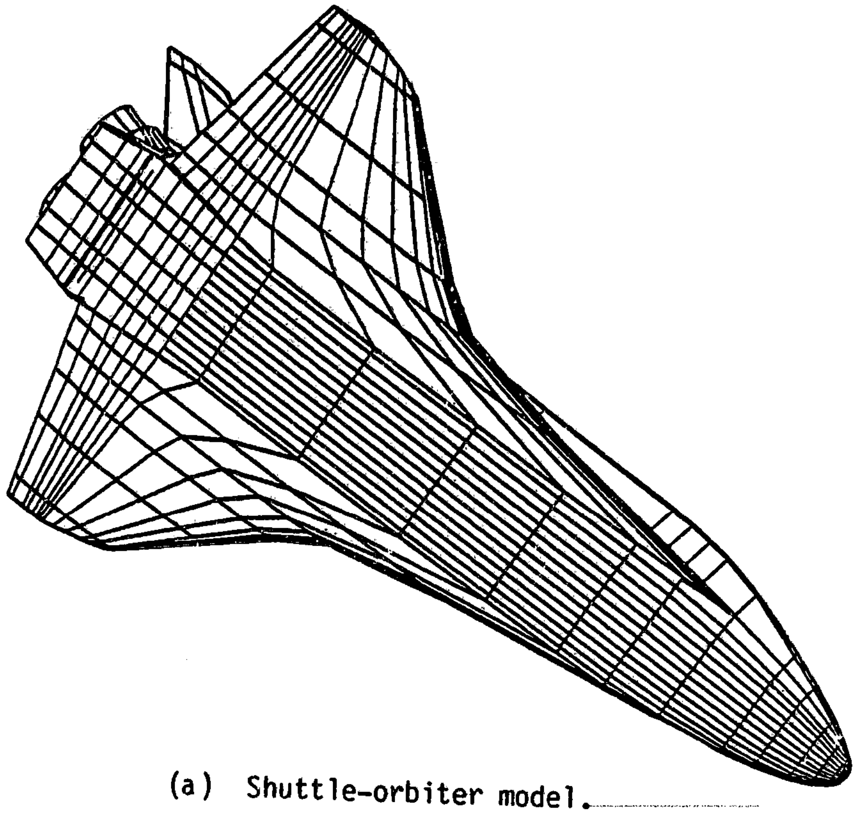

(a) Shuttle-orbiter model.

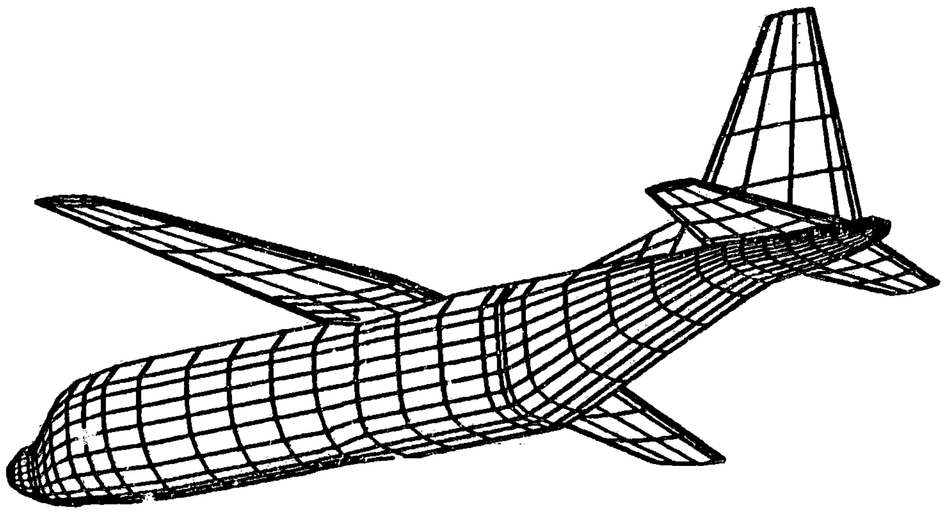

(b) C-130 Hercules aircraft model.

Figure 8. - Three-dimensional computer models constructed of quadrilateral patches.

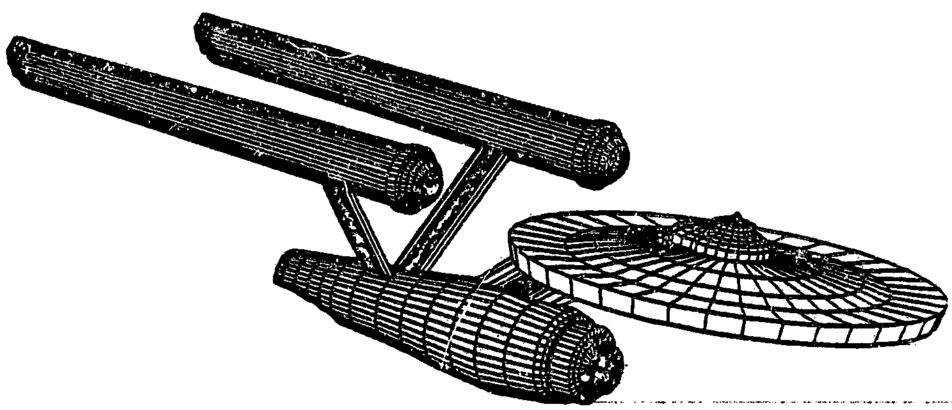

(c) Starship Enterprise model.

Figure 8. - Concluded.